ASTEROIDS

Pebbles and sand on asteroid (162173) Ryugu: In situ observation and particles returned to Earth

S. Tachibana[1,2]*, H. Sawada[2], R. Okazaki[3], Y. Takano[4], K. Sakamoto[1,2], Y. N. Miura[5], C. Okamoto[6]†, H. Yano[2], S. Yamanouchi[3], P. Michel[7], Y. Zhang[7], S. Schwartz[8,9], F. Thuillet[7]‡, H. Yurimoto[10], T. Nakamura[11], T. Noguchi[3,12], H. Yabuta[13], H. Naraoka[3], A. Tsuchiyama[14,15], N. Imae[16], K. Kurosawa[17], A. M. Nakamura[6], K. Ogawa[18], S. Sugita[1], T. Morota[1], R. Honda[19], S. Kameda[20], E. Tatsumi[1,21], Y. Cho[1], K. Yoshioka[1], Y. Yokota[2], M. Hayakawa[2], M. Matsuoka[2]§, N. Sakatani[20], M. Yamada[17], T. Kouyama[22], H. Suzuki[23], C. Honda[24], T. Yoshimitsu[2], T. Kubota[2], H. Demura[24], T. Yada[2], M. Nishimura[2], K. Yogata[2], A. Nakato[2], M. Yoshitake[2], A. I. Suzuki[25,26], S. Furuya[1,2], K. Hatakeda[25], A. Miyazaki[2], K. Kumagai[25], T. Okada[2], M. Abe[2,27], T. Usui[2], T. R. Ireland[28], M. Fujimoto[2], T. Yamada[2], M. Arakawa[6], H. C. Connolly Jr.[29,8], A. Fujii[2], S. Hasegawa[2], N. Hirata[24], N. Hirata[6], C. Hirose[30], S. Hosoda[2], Y. Iijima[2]†, H. Ikeda[2], M. Ishiguro[31], Y. Ishihara[18], T. Iwata[2,27], S. Kikuchi[2,17], K. Kitazato[24], D. S. Lauretta[8], G. Libourel[7], B. Marty[32], K. Matsumoto[33,34], T. Michikami[35], Y. Mimasu[2], A. Miura[2,27], O. Mori[2], K. Nakamura-Messenger[36], N. Namiki[33,34], A. N. Nguyen[36], L. R. Nittler[37], H. Noda[33,34], R. Noguchi[2,38], N. Ogawa[18], G. Ono[30], M. Ozaki[2,27], H. Senshu[17], T. Shimada[18], Y. Shimaki[2], K. Shirai[2], S. Soldini[39], T. Takahashi[40], Y. Takei[2,30], H. Takeuchi[2,27], R. Tsukizaki[2], K. Wada[17], Y. Yamamoto[2,27], K. Yoshikawa[30], K. Yumoto[1], M. E. Zolensky[36], S. Nakazawa[2], F. Terui[2]¶, S. Tanaka[2,27], T. Saiki[2], M. Yoshikawa[2,27], S. Watanabe[41], Y. Tsuda[2,42]

The Hayabusa2 spacecraft investigated the C-type (carbonaceous) asteroid (162173) Ryugu. The mission performed two landing operations to collect samples of surface and subsurface material, the latter exposed by an artificial impact. We present images of the second touchdown site, finding that ejecta from the impact crater was present at the sample location. Surface pebbles at both landing sites show morphological variations ranging from rugged to smooth, similar to Ryugu's boulders, and shapes from quasi-spherical to flattened. The samples were returned to Earth on 6 December 2020. We describe the morphology of >5 grams of returned pebbles and sand. Their diverse color, shape, and structure are consistent with the observed materials of Ryugu; we conclude that they are a representative sample of the asteroid.

Asteroids are small celestial bodies in the Solar System that are left over from the planet formation process. The C-type (carbonaceous) group of asteroids appear to be related to carbonaceous chondrite meteorites, which are known to contain hydrated silicates and organic matter (*1*). Such hydrated asteroids could have delivered water and organic molecules to Earth during or after its formation. Samples from C-type asteroids are predicted to contain a record of Solar System evolution (*1*). Evidence for ongoing activity on an asteroid surface, including movement and ejection of particles, has previously been inferred from analysis of particles returned to Earth from the S-type (stony) asteroid (25143) Itokawa (*2*, *3*).

The Hayabusa2 spacecraft investigated the C-type near-Earth asteroid (162173) Ryugu from June 2018 to November 2019, with the goal of determining its physical and compositional properties, collecting samples, and returning them to Earth. Ryugu is a "spinning top"–shaped rubble pile, with a mean radius of 448 ± 2 m (*4*, *5*). The surface is ubiquitously dark, with variations in reflectance spectra that are due to mixing of bluish and reddish materials (*5*, *6*). Some bright boulders are present, which could be related to spectroscopically similar S-type asteroids (*7*). The reddish color is thought to have been produced by surface alteration and space weathering of originally bluish materials during the past 10^6 to 10^7 years (*6*). Hydrous silicates are present across the surface (*8*) but are less abundant than in hydrated carbonaceous chondrites (*8*) or the B-type (bluish and spectroscopically similar to C-type) asteroid (101955) Bennu (*9*, *10*). This could be due to dehydration of originally hydrous silicates or minimal aqueous alteration of Ryugu's parent planetesimal (the original body in the early Solar System from which Ryugu formed) (*5*, *8*).

Hayabusa2 dropped the Mobile Asteroid Surface Scout (MASCOT) lander onto Ryugu, which showed that the surface is not covered with fine regolith (*11*). A ~3-cm pebble observed by using MASCOT had a thermal inertia of ~280 J m^{-2} K^{-1} $s^{-1/2}$, which is much lower than the thermal inertia of chondrites (*12*). This low thermal inertia indicates that the pebble had a high porosity, implying a low tensile strength of a few hundred kilopascals (*12*). Similarly low thermal inertia (~300 J m^{-2} K^{-1} $s^{-1/2}$) was measured for several large (>10 m) boulders and their surroundings (*13*). An artificial impact experiment was performed by using Hayabusa2's Small Carry-on Impactor (SCI), which showed that Ryugu's surface is composed of a cohesionless material, at least in part (*14*). Infrared observations of the SCI-made crater have shown that the subsurface material has spectral properties

[1]UTokyo Organization for Planetary and Space Science–Department of Earth and Planetary Science, The University of Tokyo, Tokyo 113-0033, Japan. [2]Institute of Space and Astronautical Science, Japan Aerospace Exploration Agency (JAXA), Sagamihara 252-5210, Japan. [3]Department of Earth and Planetary Sciences, Kyushu University, Fukuoka 812-8581, Japan. [4]Biogeochemistry Research Center, Japan Agency for Marine-Earth Science and Technology, Kanagawa 237-0061, Japan. [5]Earthquake Research Institute, The University of Tokyo, Tokyo 113-0032, Japan. [6]Department of Planetology, Kobe University, Kobe 657-8501, Japan. [7]Université Côte d'Azur, Observatoire de la Côte d'Azur, Centre national de la recherche scientifique, Laboratoire Lagrange, F-06304 Nice CEDEX 4, France. [8]Lunar and Planetary Laboratory, University of Arizona, Tucson, AZ 85705, USA. [9]Planetary Science Institute, Tucson, AZ 85719, USA. [10]Department of Earth and Planetary Sciences, Hokkaido University, Sapporo 060-0810, Japan. [11]Department of Earth Sciences, Tohoku University, Sendai 980-8578, Japan. [12]Division of Earth and Planetary Sciences, Kyoto University, Kyoto, Japan. [13]Department of Earth and Planetary Systems Science, Hiroshima University, Higashi-Hiroshima 739-8526, Japan. [14]Research Organization of Science and Technology, Ritsumeikan University, Kusatsu 525-8577, Japan. [15]Guangzhou Institute of Geochemistry, Chinese Academy of Sciences, Guangzhou 510640, China. [16]Polar Science Resources Center, National Institute of Polar Research, Tokyo 190-8518, Japan. [17]Planetary Exploration Research Center, Chiba Institute of Technology, Narashino 275-0016, Japan. [18]JAXA Space Exploration Center, JAXA, Sagamihara 252-5210, Japan. [19]Department of Information Science, Kochi University, Kochi 780-8520, Japan. [20]Department of Physics, Rikkyo University, Tokyo 171-8501, Japan. [21]Instituto de Astrofísica de Canarias, University of La Laguna, E-38205 Tenerife, Spain. [22]Information Technology and Human Factors, National Institute of Advanced Industrial Science and Technology, Tokyo 135-0064, Japan. [23]Department of Physics, Meiji University, Kawasaki 214-8571, Japan. [24]Aizu Research Center for Space Informatics, University of Aizu, Aizu-Wakamatsu 965-8580, Japan. [25]Marine Works Japan Ltd., Yokosuka 237-0063, Japan. [26]Department of Economics, Toyo University, Tokyo 112-8606, Japan. [27]Department of Space and Astronautical Science, The Graduate University for Advanced Studies, SOKENDAI, Hayama 240-0193, Japan. [28]School of Earth and Environmental Sciences, The University of Queensland, St Lucia, Queensland 4072, Australia. [29]Department of Geology, Rowan University, Glassboro, NJ 08028, USA. [30]Research and Development Directorate, JAXA, Sagamihara 252-5210, Japan. [31]Department of Physics and Astronomy, Seoul National University, Seoul 08826, Korea. [32]Université de Lorraine, Centre national de la recherche scientifique, Centre de Recherches Pétrographiques et Géochimiques, F-54000 Nancy, France. [33]National Astronomical Observatory of Japan, Mitaka 181-8588, Japan. [34]Department of Astronomical Science, The Graduate University for Advanced Studies, SOKENDAI, Hayama 240-0193, Japan. [35]Department of Mechanical Engineering, Kindai University, Higashi-Hiroshima 739-2116, Japan. [36]NASA Johnson Space Center, Houston, TX 77058, USA. [37]Carnegie Institution for Science, Washington, DC 20015, USA. [38]Department of Science, Niigata University, Niigata 950-2181, Japan. [39]Department of Mechanical, Materials and Aerospace Engineering, University of Liverpool, Liverpool L69 3BX, UK. [40]NEC Corporation, Tokyo 183-8501, Japan. [41]Department of Earth and Environmental Sciences, Nagoya University, Nagoya 464-8601, Japan. [42]Department of Aeronautics and Astronautics, The University of Tokyo, Tokyo 113-0033, Japan.
***Corresponding author. Email: tachi@eps.s.u-tokyo.ac.jp** †Deceased. ‡Present address: CS Group, 31506 Toulouse CEDEX 5, France. §Present address: Laboratoire d'Etudes Spatiales et d'Instrumentation en Astrophysique, Observatoire de Paris, 92195 Meudon, France. ¶Present address: Department of Mechanical Engineering, Kanagawa Institute of Technology, Kanagawa 243-0292, Japan.

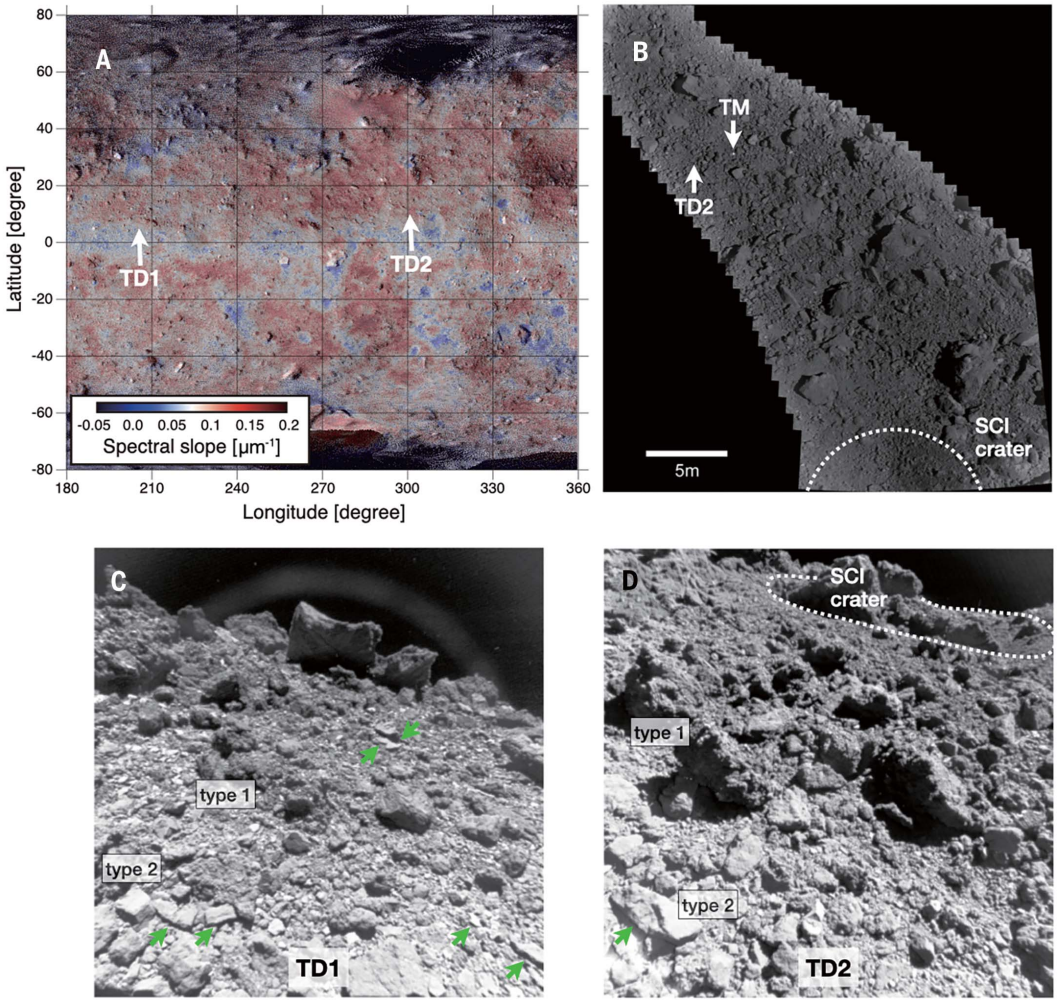

Fig. 1. Hayabusa2 touchdown locations and Ryugu surface properties. (**A**) Global map of the spectral slope, which is indicated by the color bar, superimposed on a *v*-band image map. The spectral slope is measured between the *b*-band (0.48 μm) and the *x*-band (0.86 μm) (*5*, *6*). The white arrows indicate the locations of the first touchdown (TD1) and the second touchdown (TD2). (**B**) Composite map of the TD2 site, assembled from images taken by a wide-angle optical navigation camera (ONC-W1). Also visible are the locations of a target marker (arrow labeled TM) that was used for spacecraft navigation and the crater produced by the SCI experiment (dotted arc, diameter of ~18 m) (*19*). (**C** and **D**) Images of the areas surrounding the TD1 and TD2 sites, respectively, taken by another wide-angle optical navigation camera (ONC-W2). Examples of flattened boulders and pebbles are indicated with green arrows. Labels indicate type 1 and type 2 boulders, which have rugged and smooth surfaces, respectively (*5*). The SCI crater (*14*) is visible (dotted ellipse) in the image of the TD2 site. The arch-like feature above the surface in (C) is an artifact.

similar to, but distinct from, those of the surface (*15*). The crater and excavated material have a slightly higher abundance of hydrated silicates, reflecting the extent of aqueous alteration that occurred on Ryugu's parent planetesimal (*15*).

Sample-collection operations

Hayabusa2 made its first landing [designated touchdown one (TD1)] on 2019 February 21, during which it collected samples of the surface (*6*). The second landing (TD2) occurred on 2019 July 11, close to the crater made by the SCI, to collect impact ejecta, i.e., subsurface samples (Fig. 1). The two landing locations appeared similar in remote imaging, being covered with boulders and pebbles (Fig. 1). The two types of boulder commonly observed on Ryugu's surface [rugged type 1 and smooth type 2 (*5*)] are found at both locations. In both landing operations, a 5-g tantalum projectile was fired through the sampler horn at ~300 ± 30 m s^{-1} (*1*, *16*, *17*) when the horn touched the surface, lifting material into the collector.

The TD2 location hosts fine particle aggregates, observed on the surface of a smooth type 2 boulder (Fig. 2A), which were not identified in proximity images of TD1 or other surface locations (*6*). These particles did not strongly adhere to the boulder, being blown off by the subsequent ascent thruster firing (Fig. 2B). We infer that the fine particles are geologically recent and, most likely, ejecta from the SCI crater. Images of the impact event show that part of the ejecta curtain fell back on Ryugu's surface, with simulations predicting that the TD2 site was covered with SCI ejecta excavated from a depth of ~1 m below the surface (*18*, *19*). The estimated sizes of ejecta particles range from 1 mm to several decimeters (*18*). This is consistent with the observed particles on the boulder (Fig. 3). We conclude that the TD2 sample location was covered with ejecta excavated from Ryugu's subsurface by the SCI experiment. Sample-collection analog experiments that were performed in Earth gravity indicate that ~50% of the collected particles were taken from depths <1.5 mm from the surface (fig. S3) (*20*). Collection under microgravity should access greater depths; nevertheless, we expect the samples collected during TD2 to include some SCI ejecta. Spectroscopy of the SCI crater and its surroundings revealed only small differences (*15*), so the identification of subsurface materials in the collected sample requires other analysis methods.

During both landings, the motions of particles kicked up by the sample projectiles and thruster firings were observed with a small monitor camera head (CAM-H) (Fig. 3 and movie S1) (*20*). One second after the projectile firing at TD1, ~10 particles were identified beneath or nearby the sampler horn (Fig. 3C). After another second, the number of particles increased to ~20 in the next image (Fig. 3D), of which 3 particles were moving toward CAM-H. We estimate the ejection angle and velocity of these particles as ~50° to 60° and 1 to 2 m s^{-1}, respectively (*20*). Their ejection angle is within the range measured in projectile experiments in Earth gravity (40° to 60°; fig. S2) (*20*) and consistent with the most frequent angle range (48° to 54°) in the Hayabusa2 sampling simulations (*21*). We conclude that these particles

are ejecta produced by the projectile impact. The ejected particles identified near the rocket coupling ring (an assembly used during the spacecraft launch) were centimeter-sized (Fig. 3). Centimeter-sized pebbles were also found in proximity images of the TD1 site (*6*) and at different surface locations observed by the lander MASCOT (*11*) and the MINERVA-II (Micro Nano Experimental Robot Vehicle for Asteroid 2) Rover-1A (Fig. 2). The data from MINERVA-II Rover-1A also showed centimeter-sized particles that were disturbed by its hop across the surface (Fig. 2D) (*20*). This suggests that centimeter-sized pebbles, which do not strongly adhere to larger cobbles and boulders, are present over the surface of Ryugu.

We estimate the total mass of the three ejecta particles observed in Fig. 3 as 0.3 to 3 g, assuming spherical particles with a diameter of 0.5 to 1 cm and bulk density of ~2 g cm^{-3}. If all the ejecta particles in Fig. 3 (~20 in number) have the same ejection velocity as the three particles observed moving toward CAM-H, the total amount of ejecta with an ejection velocity of ~1 m s^{-1} would be ~2 to 20 g. Numerical simulations of the Hayabusa2 sample process, which assume a cohesionless granular bed consisting of grains with an average diameter of 0.5 cm, predicted that the total ejecta mass is about an order of magnitude larger than the mass of ejecta with a velocity of ~1 m s^{-1} (*21*). We therefore estimate the total ejecta mass as 20 to 200 g. The simulations also predicted that ~0.5% of the total ejecta particles are retained in the sample catcher, which is located above the sampler horn (*21*). This leads to an estimated total collected mass of 0.1 to 1 g for TD1, which meets the 0.1-g requirement for returned sample analysis (*1*, *16*). Laboratory experiments conducted under Earth gravity by using 1-mm glass spherules with little cohesion force showed that 150 to 250 mg of samples can be collected after projectile firing (fig. S1) (*20*), which was expected to be increased up to an order of magnitude under microgravity conditions (*16*). Because the surface materials on Ryugu are not strongly held to the surface by cohesive forces (*14*), we regard this experiment as an appropriate analog of the sample-collection operation on Ryugu.

In the CAM-H images taken during TD2 (Fig. 3 and movies S2 and S3), dust-like ejecta appear from beneath the sampler horn (Fig. 3), followed by the ejection of numerous larger particles, which is likely due to the projectile firing. We interpret this dust as ejecta with slow velocities or originating from deeper into the surface that did not enter the sampler horn. Three particles visible in Fig. 3 are ~1 to 2 cm in diameter, which suggests that loosely packed, movable, centimeter-sized pebbles were present at the TD2 location. The CAM-H images suggest that the amount of material collected during TD2 was similar to the amount collected during TD1.

Spacecraft ascent

CAM-H continued to take images of flying particles during the ascent after the two landing operations (Fig. 4). Flying particles are visible as objects moving relative to the surface in multiple sequential images (movies S1 and S2). Because no such flying particles were observed during the spacecraft descent, we interpret these particles as ejecta either due to the projectile impact or lifted by the spacecraft thruster firing. Images from a wide-angle optical navigation camera showed boulders moving on the surface because of the thruster operation during TD1 (*6*), so we infer that the thruster triggered the ejection of most of the pebbles as well. Numerous millimeter-sized particles were also observed during the TD2 ascent operation (Fig. 4), which indicates the presence of more small particles at the TD2 location than at the TD1 location, which were presumably the SCI ejecta.

The flying pebbles show two morphological types: rugged particles and particles with smooth faces (Fig. 4 and fig. S4). These two types are consistent with the morphological variations that were observed within surface boulders observed by the spacecraft (*5*) and the MASCOT lander (*11*). We determined the three-dimensional shapes of flying pebbles for those visible in multiple two-dimensional projections (from different angles) in the CAM-H images. We define *L* and *I* as the maximum and minimum caliper

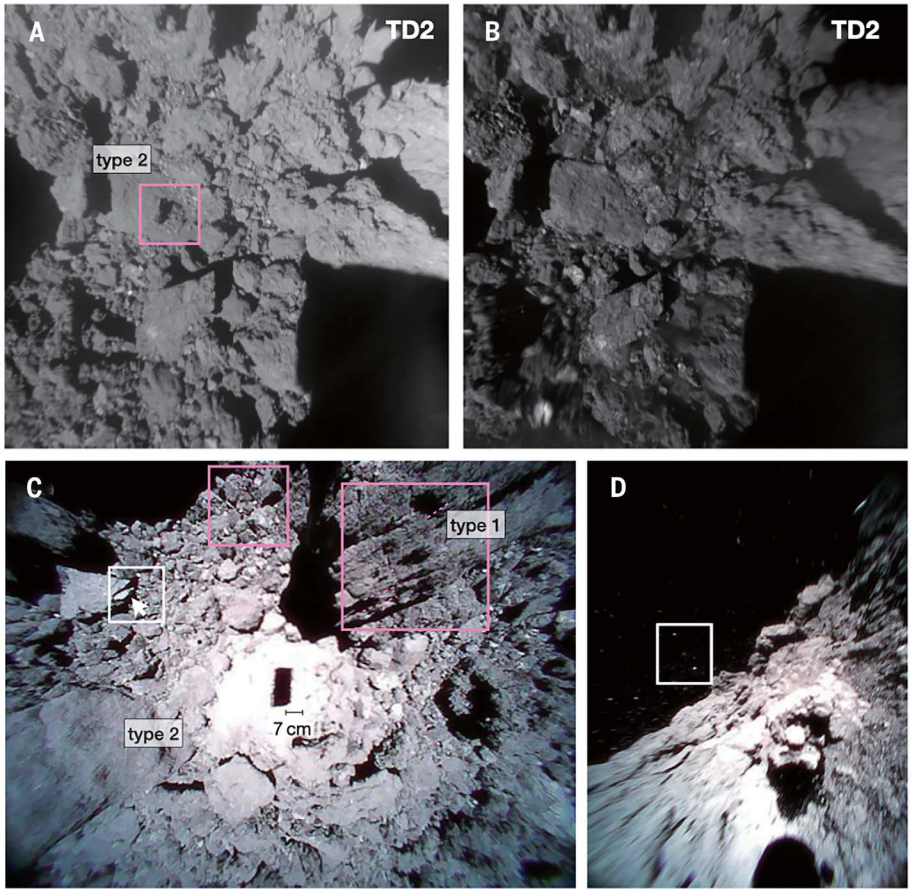

Fig. 2. Pebbles and boulders observed on Ryugu's surface. (**A**) ONC-W1 image taken 2 s before TD2. Fine particles are visible (within the pink box, which measures ~20 by 20 cm) on the surface of a smooth type 2 boulder (*5*). (**B**) Same area as shown in (A), taken during the ascent after TD2. The fine particles on the smooth type 2 boulder were blown off by the thruster firing. (**C**) Image of the surface taken by the MINERVA-II Rover-1A during its hopping operation on 2018 September 28. The shadow of the rover (~7 cm long) is visible in the center of the image. Numerous decimeter- to centimeter-sized pebbles are visible. Boulders with layered structure (pink boxes with layers indicated by dotted lines) are observed, along with a boulder from which a flattened piece seems to be peeling (arrow in the white box). Both type 1 and type 2 boulders are present in this region (labeled). (**D**) Image taken during a hop of MINERVA-II Rover-1A on 2018 October 16. Ejected centimeter-sized pebbles are visible within the white box.

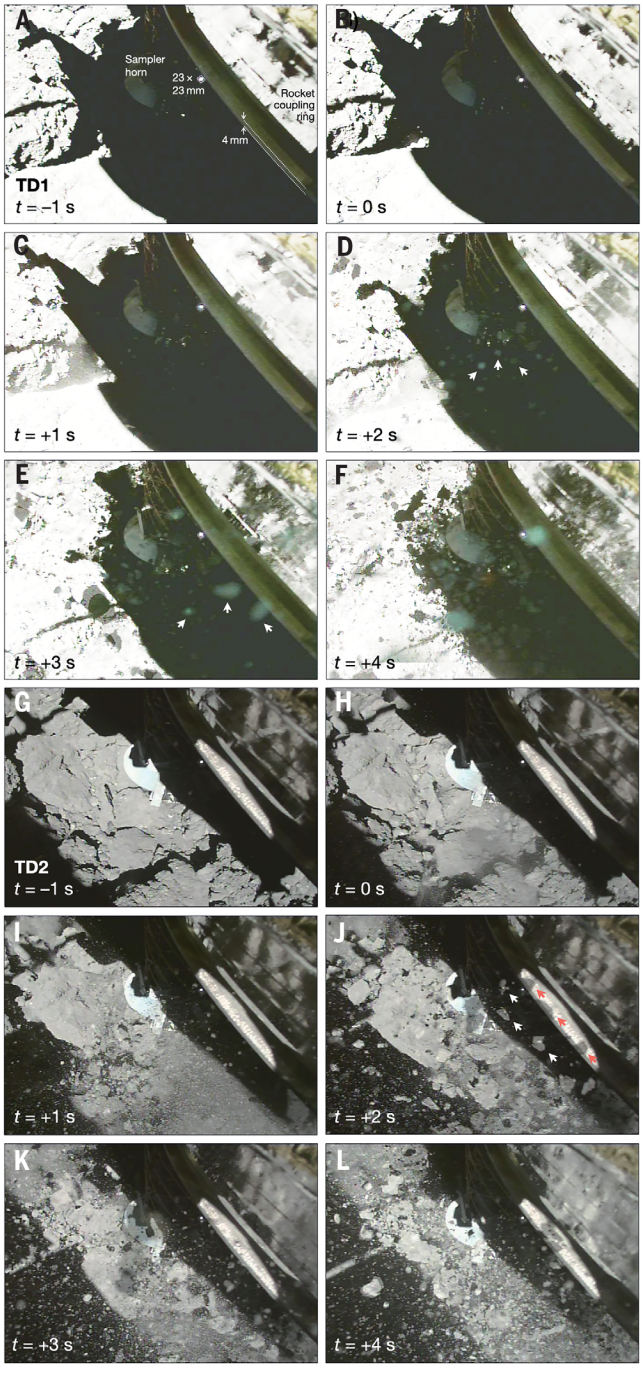

Fig. 3. CAM-H images of the TD1 and TD2 sample acquisition processes. (**A** to **F**) TD1 operation. The lower left of each panel indicates the time *t* from projectile firing, ranging from −1 to +4 s. Ejecta particles are visible after *t* = 0. A reflection plate for a laser range finder (23 mm by 23 mm) on the sampler horn and the rim of the rocket coupling ring (4 mm; distance between arrows) are labeled as size references. The white arrows in (D) and (E) indicate the same group of particles moving toward CAM-H. (**G** to **L**) Equivalent images of TD2. Three particles, indicated with white arrows in (J), are also seen as mirror images reflected on the rocket coupling ring (red arrows).

lengths—the distance between two parallel lines tangential to the surface—of the maximum-area projection of each particle and *S* as the smallest dimension measured in the minimum-area projection (fig. S5) (*20*, *22*). The shortest axis to longest axis (*S*/*L*) and intermediate axis to longest axis (*I*/*L*) ratios of the particles (Fig. 4 and tables S1 and S2) show that there is a fraction of elongated block-like flat particles on the surface. The 67 particles have a bimodal distribution centered at (*S*/*L*, *I*/*L*) of (0.53, 0.69) and (0.35, 0.48) (Fig. 5), which means that two shape types are present in the population of surface pebbles, which we refer to as "subequant" and "elongated block" (*23*). Pebbles and small boulders with a shape that is both elongated and flat are found at both landing locations (Fig. 1). This suggests that the bimodal distribution of pebble shapes is indigenous to Ryugu's surface. However, because such a bimodal distribution is not found for boulders larger than 5 m (*24*), we conclude that this shape variation results from boulder fragmentation or foliation (Fig. 2) (*5*). This elongated and flat morphology is not typical among clasts (embedded fragments) in carbonaceous chondrite meteorites but is similar to the texture of clasts in shocked hydrated carbonaceous chondrites (*25*–*28*). Some of the latter show a high density of parallel fractures that formed because of sudden volatile loss during the release of shock pressure (*28*).

During the TD1 ascent operation, CAM-H observed a centimeter-sized pebble that passed between the camera and the rocket coupling ring (Fig. 4, C and D). The pebble hit the spacecraft; then 4 s later, a smaller particle (~4 mm in size) appeared from the spacecraft side (Fig. 4E). Because no other particles coming from the spacecraft side were observed during the TD1 and TD2 operations, the ~4-mm–sized particle is likely to be a fragment of this centimeter-sized pebble that resulted from its impact with the spacecraft. The CAM-H images from the ascending spacecraft (~1 m s^{-1}) suggest that the relative velocity of the pebble to the spacecraft was ~0.1 m s^{-1}. Because fragmentation of typical carbonaceous chondrite material requires an impact velocity of >1 m s^{-1} (*20*, *29*), this implies that the tensile strength of the pebble is much lower than that of typical chondrites (fig. S6) (*17*, *20*). The highly porous material identified on the surface (*30*) could be of similar composition to the fragile pebble. Alternatively, the pebble might have contained a crack (or cracks), such as the one that was observed on a boulder by the MINERVA-II Rover-1A (Fig. 2).

Samples returned to Earth

Hayabusa2 left Ryugu in November 2019. On 6 December 2020, the reentry capsule containing the samples was delivered to Woomera, South Australia. After transfer to a clean room, the sample chambers were opened and found to contain ~5 g of material (*31*). This is ~50 times more than the mission minimum requirement of 0.1 g (*1*, *16*). The samples recovered from chamber A (24 cm^3) of the sample catcher, which was used for the storage of TD1 samples, weigh ~3 g. This mass is consistent with the estimate above based on CAM-H images. We therefore conclude that the sample in

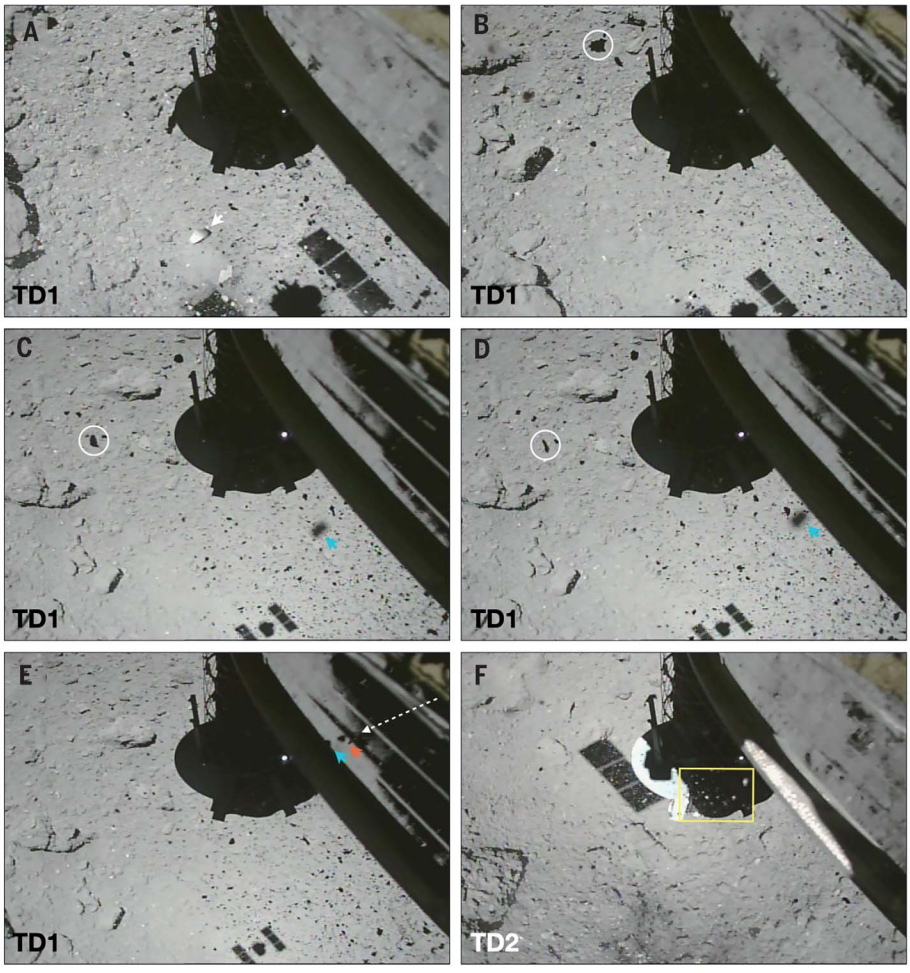

Fig. 4. CAM-H images of flying particles during the ascent operations. (**A**) Particle with smooth faces indicated with a white arrow. (**B**) Rugged particle indicated with a white circle. (**C** and **D**) Flat particle (white circle) and particle that appears to have hit the spacecraft (blue arrow). (**E**) Particle coming from the spacecraft side indicated with a blue arrow. Its mirror image is seen on the rocket coupling ring (red arrow). The particle's direction of movement is shown with a white dotted arrow. (**F**) Millimeter-sized particles (within the yellow box) observed after TD2. Movies S1 and S2 show the full footage of these operations, in which the particle movements are visible. (A) to (E) are from TD1, and (F) is from TD2.

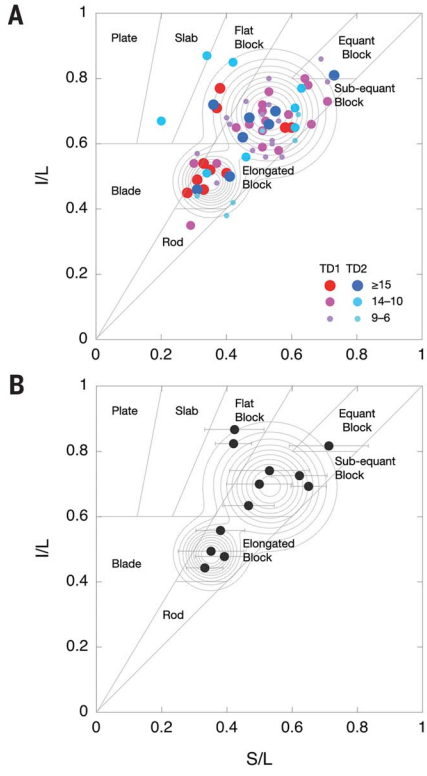

Fig. 5. Shape parameters of flying particles observed during touchdown operations and particles returned to Earth. (**A**) Properties of particles observed during TD1 and TD2 operations. *S/L* is the ratio of the shortest axis to the longest axis, and *I/L* is the ratio of the intermediate axis to the longest axis (*25*). Contours indicate the probability distribution function of 67 particles, assuming a bimodal distribution (*25*). (**B**) Properties of returned samples, six particles each from chambers A and C (*25*), overlain on the same contours from (A). The distribution is similar. Data for all the particles in both panels are listed in tables S1 to S3.

chamber A was lifted by the projectile firing, which worked efficiently to collect asteroid surface regolith. This is unlike the particles returned from the asteroid Itokawa by the original Hayabusa spacecraft, as its projectile failed to fire, which complicated interpretation of the samples (*2*). Chamber C (12 cm^3) of the sample catcher, which was used for samples from TD2, contained ~2 g. This is also consistent with the estimate above from the CAM-H images, which suggests that chamber C samples are also the ejecta from the projectile firing. Unlike TD1, the TD2 sample likely includes material from the subsurface that was excavated by the SCI impact.

We compare the properties of the returned particles to the constraints derived above from the sample collection images. In both chambers of the sample container, millimeter-sized sand and nearly centimeter-sized pebbles were found, along with submillimeter-sized fine powder. The grain size variation is consistent with expectations derived from the surface observation by the MASCOT lander (*11*), MINERVA-II rovers, Hayabusa2 cameras (Figs. 2 to 4), and polarimetric observations from Earth (*32*). All the particles in the two chambers appeared black (Fig. 6), which is consistent with the color and albedo of Ryugu's boulders (*5*, *6*). The sizes of the collected particles are consistent with the ejecta observed during each landing operation (Fig. 3). The largest grains from chamber A are ~5 mm in size, whereas there are three pebbles larger than 5 mm from chamber C (Fig. 6 and table S3). The longest dimension of the largest pebble in chamber C is 10.3 mm, which is close to the maximum size obtainable by the Hayabusa2 sampler (*16*, *21*). The presence of these large pebbles in chamber C, despite the smaller total mass, can be explained either by projectile destruction of a larger rock or the scoop-up component of the sampler horn, which was designed to pick up surface pebbles (*16*). Millimeter-sized fine grains and submillimeter-sized sand particles were also found in chamber C, which are likely to include subsurface material, as observed on a boulder (Fig. 2A). Chamber B, which was not used for either landing operation, is located between chambers A and C. A small number of fine particles (smaller than 1 mm) were found in this chamber. This shows that no extensive mixing of particles occurred through the gaps between the chambers during the return to Earth or capsule recovery (*16*). We are therefore confident that the pebbles and sand in chambers A

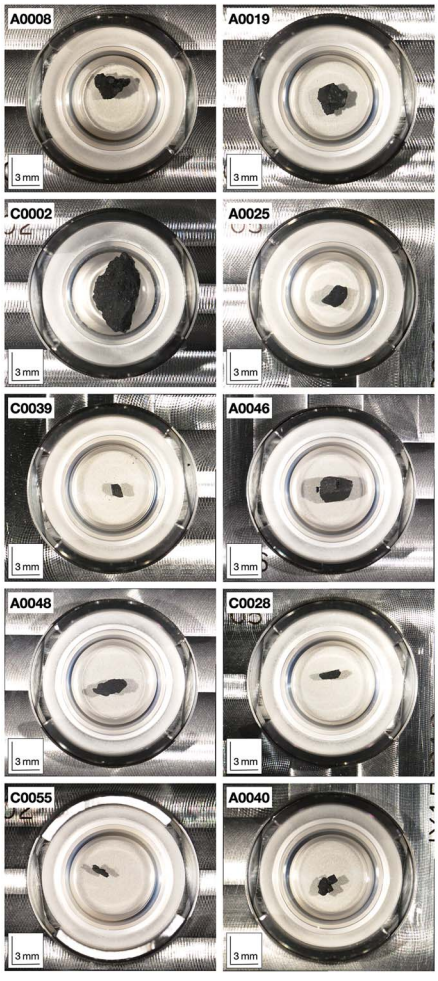

Fig. 6. Microscope images of particles returned to Earth inside the sample container. Particles cataloged as A0008, A0019, A0046, A0048, A0069, and A0083 are from chamber A of the sample container used for TD1. C0002, C0004, C0013, C0019, C0028, and C0055 are from chamber C of the sample container used for TD2. The particles A0008, A0019, A0069, A0083, and C0002 have rugged surfaces, whereas A0046 and C0019 have smooth surfaces. The particles A0048, C0028, and C0055 show elongated blocklike morphologies. Particles were mounted on individual sample holders in a nitrogen atmosphere and are lit from the left and right simultaneously.

and C are the samples acquired in the TD1 and TD2 operations, respectively.

More than 200 pebbles (1 to 10 mm in size) from chambers A and C were individually removed and observed under an optical microscope (Fig. 6). These pebbles show morphological variations: Grains with rugged surface and with smooth surfaces are observed (Fig. 6), which is consistent with the flying pebbles observed during the TD1 and TD2 operations. Although only a few particles have been measured, the elongated block-like pebbles in the collected sample (Fig. 6) have S/L and I/L ratios (Fig. 5B) that are consistent with those of the flying particles observed at Ryugu (Fig. 5A).

Many returned particles feature curved and straight cracks. Pebbles with a smooth surface could be fragments of particles with straight cracks, possibly formed by shock or thermal fatigue (*33*). The common presence of cracks in returned pebbles implies that the small thermal inertia of surface boulders (*12*, *13*) is probably due, at least in part, to cracks or fractures in their interior. Microcracks or microporosity could also be responsible for the low thermal inertia.

The color, shape, surface morphology, and structure of the returned pebbles and sand match those of Ryugu's surface material observed from the spacecraft. We therefore conclude that the pebbles and sand inside chambers A and C are representative samples of Ryugu at two surface sites, without substantial alteration during the sample collection and return to Earth. The variations in physical properties among the pebbles and sand, which were not expected before spacecraft arrival at the asteroid, reflect the geological history of Ryugu (*1*).

REFERENCES AND NOTES

1. S. Tachibana *et al.*, *Geochem. J.* **48**, 571–587 (2014).
2. A. Tsuchiyama *et al.*, *Science* **333**, 1125–1128 (2011).
3. K. Nagao *et al.*, *Science* **333**, 1128–1131 (2011).
4. S. Watanabe *et al.*, *Science* **364**, 268–272 (2019).
5. S. Sugita *et al.*, *Science* **364**, 252 (2019).
6. T. Morota *et al.*, *Science* **368**, 654–659 (2020).
7. E. Tatsumi *et al.*, *Nat. Astron.* **5**, 39–45 (2021).
8. K. Kitazato *et al.*, *Science* **364**, 272–275 (2019).
9. D. S. Lauretta *et al.*, *Nature* **568**, 55–60 (2019).
10. V. E. Hamilton *et al.*, *Nat. Astron.* **3**, 332–340 (2019).
11. R. Jaumann *et al.*, *Science* **365**, 817–820 (2019).
12. M. Grott *et al.*, *Nat. Astron.* **3**, 971–976 (2019).
13. T. Okada *et al.*, *Nature* **579**, 518–522 (2020).
14. M. Arakawa *et al.*, *Science* **368**, 67–71 (2020).
15. K. Kitazato *et al.*, *Nat. Astron.* **5**, 246–250 (2021).
16. H. Sawada *et al.*, *Space Sci. Rev.* **208**, 81–106 (2017).
17. R. Okazaki *et al.*, *Space Sci. Rev.* **208**, 107–124 (2017).
18. K. Wada *et al.*, *Astron. Astrophys.* **647**, A43 (2021).
19. R. Honda *et al.*, *Icarus* **366**, 114530 (2021).
20. Materials and methods are available as supplementary materials.
21. F. Thuillet, P. Michel, S. Tachibana, R.-L. Ballouz, S. R. Schwartz, *Mon. Not. R. Astron. Soc.* **491**, 153–177 (2019).
22. G. H. Bagheri, C. Bonadonna, I. Manzella, P. Vonlanthen, *Powder Technol.* **270**, 141–153 (2015).
23. S. J. Blott, K. Pye, *Sedimentology* **55**, 31–63 (2008).
24. T. Michikami *et al.*, *Icarus* **331**, 179–191 (2019).
25. M. E. Zolensky *et al.*, *Geochim. Cosmochim. Acta* **61**, 5099–5115 (1997).
26. A. E. Rubin, *Geochim. Cosmochim. Acta* **90**, 181–194 (2012).
27. R. D. Hanna, R. A. Ketcham, M. E. Zolensky, W. M. Behr, *Geochim. Cosmochim. Acta* **171**, 256–282 (2015).
28. T. Nakamura *et al.*, Irradiation-energy dependence of the spectral changes of hydrous C-type asteroids based on 4 keV and 20 keV He exposure experiments of Murchison CM chondrite, 51st Lunar and Planetary Science Conference, 16 to 20 March 2020, The Woodlands, TX, Abstract 1310.
29. M. Setoh, A. M. Nakamura, N. Hirata, K. Hiraoka, M. Arakawa, *Earth Planets Space* **59**, 319–324 (2007).
30. N. Sakatani *et al.*, *Nat. Astron.* **5**, 766–774 (2021).
31. T. Yada *et al.*, *Nat. Astron.* 10.1038/s41550-021-01550-6 (2021).
32. D. Kuroda *et al.*, *Astrophys. J. Lett.* **911**, L24 (2021).
33. G. Libourel *et al.*, *Mon. Not. R. Astron. Soc.* **500**, 1905–1920 (2021).

ACKNOWLEDGMENTS

Hayabusa2 was developed and built under the leadership of JAXA, with contributions from the German Aerospace Center and the Centre National d'Études Spatiales (CNES) and in collaboration with NASA and other universities, institutes, and companies in Japan. The sampler system was developed by JAXA, The University of Tokyo, Hokkaido University, Kyushu University, Japan Agency for Marine-Earth Science and Technology, and other universities, institutes, and companies in Japan. **Funding:** S. Tachibana acknowledges JSPS KAKENHI Grant (JP 20H05846). S.W. acknowledges JSPS KAKENHI Grant (17H06459 and 19H01951). P.M., B.M., Y.Z., F. Thuillet, and G.L. acknowledge the French space agency CNES. P.M. and Y.Z. acknowledge funding from the European Union's Horizon 2020 research and innovation program under grant agreement no. 870377 (project NEO-MAPP), from the Université Côte d'Azur "Individual grants for young researchers" program and from Academies of Excellence: Complex Systems and Space, Environment, Risk, and Resilience, part of the IDEX JEDI of Université Côte d'Azur. B.M. acknowledges funding from the European Research Council (grant agreement no. 695618). **Author contributions:** S. Tachibana. coordinated coauthor contributions; led the sampler development with H. Sawada; performed data analyses, and interpretations; and wrote the paper, with contributions from H. Sawada, R.O., Y. Takano, K. Sakamoto, and H. Yano. Sampler development and operation: H. Sawada, R.O., Y. Takano., K. Sakamoto, Y.N.M., C.O., H. Yano, S.Y., T. Noguchi, T. Nakamura, A.T., N.I., K. Kurosawa, and A.M.N.; CAM-H operation: H. Sawada and K.O.; ONC data acquisition and reduction: S. Sugita, R.H., T. Morota, Y. Iijima, S. Kameda, H. Sawada, E.T., C. Honda, Y. Yokota, M. Yamada, T. Kouyama, N.S., K.O., H. Suzuki, K. Yoshioka, M.H., Y.C., M.I., A. Miura, and M.M.; MINERVA-II rovers operation: T. Yoshimitsu, T. Kubota, and H.D.; capsule retrieval operation and curation: S.N., M.F., T. Yamada, T.R.I., H. Sawada, R.O., K. Sakamoto, Y. Takano, Y.N.M., H. Yano, M.N., K. Yogata, A.N., M. Yoshitake, A.I.S., S.F., K.H., A. Miyazaki, K. Kumagai, T.O., M. Abe, H. Yurimoto, T.U., and K.N.-M.; landing site characterization: Y. Tsuda, S.W., T. Saiki, S. Kikuchi, N.O., Y. Yamamoto, Y.S., K. Shirai, N.H. (Kobe), K.O., K. Kitazato, N.H. (Aizu), K.W., H. Yabuta, Y. Ishihara, R.N., T. Morota, N.S., K.M., H. Senshu, R.H., E.T., Y. Yokota, C. Honda, T. Michikami, M.M., and A.M.; interpretation and writing contribution: S. Sugita, Y. Takano, P.M., Y.Z., S. Schwarz, F. Thuillet, H. Yurimoto, T. Nakamura, T. Noguchi, H. Yabuta, H. Naraoka, A.M.N., K. Kitazato, T. Morota, T. Michikami, S. Kameda, E.T., T. Yoshimitsu, T. Yada, T.O., T.U., T.R.I., M.F., H.C.C., S. Hasegawa, D.S.L., G.L., B.M., A.N.N., L.R.N., K.W., K. Yumoto, M.E.Z.; spacecraft science operations: S. Tanaka, M. Yoshikawa, T.I., Y. Yamamoto, K.M., M. H., T.O., R.N., Y.S., N.S., H.N., M.M., H. Yano, R.T., M.O., F. Terui, N.O., H. Sawada, S. Kikuchi, H.T., G.O., Y.M., K. Yoshikawa, T.T., Y. Takei, A.F., C. Hirose, S.N., S. Hosoda, O.M., T. Shimada, S. Soldini, T. Saiki, S.W., and Y. Tsuda; project administration: S.W., M. Yoshikawa, S. Tachibana, K. Kitazato, S. Sugita, T.O., N.N., M. Arakawa, M. Abe, H.I., S. Tanaka, S.N., F.T., T. Saiki, and Y. Tsuda. All authors discussed the results and commented on the manuscript. **Competing interests:** The authors declare no competing interests. **Data and materials availability:** All images and data used in this study are available at the JAXA Data Archives and Transmission System (DARTS) at www.darts.isas.jaxa.jp/pub/hayabusa2/paper/sample/Tachibana_2022/. Other data from the mission are available at the DARTS archive www.darts.isas.jaxa.jp/planet/project/hayabusa2/ and on the Small Bodies Node of the NASA Planetary Data System https://pds-smallbodies.astro.umd.edu/data_sb/missions/hayabusa2/. The samples of Ryugu are curated by the JAXA Astromaterials Science Research Group; distribution for analysis is through an Announcement of Opportunity available at https://jaxa-ryugu-sample-ao.net. Our particle size and shape measurements are listed in tables S1 to S3.

SUPPLEMENTARY MATERIALS

science.org/doi/10.1126/science.abj8624
Materials and Methods
Figs. S1 to S7
Tables S1 to S3
References (*34*–*41*)
Movies S1 to S4

7 June 2021; accepted 25 January 2022
Published online 10 February 2022
10.1126/science.abj8624